Regulation of Solute Flux through Plasmodesmata in the Root Meristem[1][W][OA]

Heidi L. Rutschow, Tobias I. Baskin, and Eric M. Kramer*

Physics Department, Simon's Rock College, Great Barrington, Massachusetts 01230 (H.L.R., E.M.K.); and Biology Department, University of Massachusetts, Amherst, Massachusetts 01003 (H.L.R., T.I.B.)

Plasmodesmata permit solutes to move between cells nonspecifically and without having to cross a membrane. This symplastic connectivity, while straightforward to observe using fluorescent tracers, has proven difficult to quantify. We use fluorescence recovery after photobleaching, combined with a mathematical model of symplastic diffusion, to assay plasmodesmata-mediated permeability in the Arabidopsis (*Arabidopsis thaliana*) root meristem in wild-type and transgenic lines, and under selected chemical treatments. The permeability measured for the wild type is nearly 10-times greater than previously reported. Plamodesmal permeability remains constant in seedlings treated with auxin (30 nM indoleacetic acid for 2 and 24 h; 100 nM indoleacetic acid for 2 h); however, permeability is diminished in two lines previously reported to have impaired plasmodesmal function as well as in wild-type seedlings treated for 24 h with 0.6 mM tryptophan. Moreover, plasmodesmal permeability is strongly altered by applied hydrogen peroxide within 2 h of treatment, being approximately doubled at a low concentration (0.6 mM) and nearly eliminated at a higher one (6 mM). These results reveal that the plasmodesmata in the root meristem carry a substantial flux of small molecules and that this flux is subject to rapid regulation.

Plasmodesmata are plasma membrane-lined channels that cross the cell wall and connect the cytoplasm of adjacent cells (Maule, 2008; Zambryski, 2008). In tissues where the plasmodesmata are open, they give rise to a cytoplasmic continuum called the symplast. The connectivity of the symplast has been studied qualitatively by observing the movement of small fluorescent probes like fluorescein (Duckett et al., 1994) or fluorescent proteins like GFP (Kim and Zambryski, 2005). These studies have revealed that symplastic connectivity gradually declines as cells differentiate and pass from the meristem to mature tissues (Duckett et al., 1994; Kim and Zambryski, 2005). They have also revealed that plant organs contain distinct domains separated from one another by barriers to symplastic connectivity. Symplastic domains occur in meristems, where they are correlated with specific tissues and developmental events (Oparka et al., 1994; Rinne and van der Schoot, 1998), and in mature tissues, where symplastic communication does not cease entirely (Erwee and Goodwin, 1985).

Symplastic domains are believed to play important roles in growth and development. Open plasmodesmata presumably allow the passive movement of nutrients and water to sustain metabolism and growth in cells located far from the mature xylem and phloem (Bret-Harte and Silk, 1994). In addition, transcription factors and other macromolecules can pass through plasmodesmata via active transport to regulate development noncell autonomously (Lucas et al., 1995; Nakajima et al., 2001). While the role of plasmodesmal macromolecular transport has been intensively studied, the relevance of plasmodesmal solute transport has received less attention, particularly in the past decade. Even though water and some physiologically important solutes can cross the membrane via specific transporter proteins, the flux of small molecules moving through plasmodesmata is expected to include water, nutrients, hormones, and second messengers. Despite this, we know little about the magnitude of solute fluxes through plasmodesmata and to what extent these fluxes are subject to regulation (Robards and Lucas, 1990; Schulz, 1999).

Flux has typically been characterized by estimating a size exclusion limit, defined as the maximum M_r of a probe able to pass through plasmodesmata. Through numerous experiments, this characterization has shown that the size exclusion limit of small solutes is approximately 1 kD and that solute flux through plasmodesmata is passive and nonselective. In other words, the flux of a small solute through plasmodesmata is governed by the effective size of the molecule and the concentration gradient between adjacent cells.

While the size exclusion limit is a useful number, it provides only a binary (yes or no) measure of molec-

[1] This work was supported by a grant from the National Science Foundation (grant no. IOS 0815453 to E.M.K. and T.I.B.).

* Corresponding author; e-mail ekramer@simons-rock.edu.

The author responsible for distribution of materials integral to the findings presented in this article in accordance with the policy described in the Instructions for Authors (www.plantphysiol.org) is: Eric M. Kramer (ekramer@simons-rock.edu).

[W] The online version of this article contains Web-only data.

[OA] Open Access articles can be viewed online without a subscription.

www.plantphysiol.org/cgi/doi/10.1104/pp.110.168187

ular movement. A complete picture requires information about the magnitude of the molecular flux, that is, the number of molecules moving through the channel per unit time. A flux may be observed qualitatively using a variety of techniques, including electrical coupling, the movement of microinjected dyes, and the photobleaching of dyes (Tucker et al., 1989; Robards and Lucas, 1990; Schulz, 1999). However, only a handful of studies have attempted to quantify the molecular flux, either through an individual plasmodesma or across a given cell wall (Tucker et al., 1989; Goodwin et al., 1990). These studies used microinjection, and so suffer from the drawback that they might trigger changes in the plasmodesmal conductivity because of a wound response (Radford and White, 2001). A second limitation of published studies is that experimental and theoretical challenges have encouraged a focus on large cells in simple tissues—for example, filamentous stamenal hairs or aquatic leaves just two cell layers thick. To our knowledge, plasmodesmal flux has never been quantified in a fully three-dimensional tissue, such as a meristem.

In this article, we present an assay based on fluorescence recovery after photobleaching to quantify the plasmodesmal permeability in the root meristem of Arabidopsis (*Arabidopsis thaliana*). The protocol avoids possible complications due to microinjection by application of carboxyfluorescein (CF) diacetate, which is membrane permeable and nonfluorescent. Once in the cytoplasm, the acetate groups are cleaved by endogenous esterases to yield fluorescent CF, which is not membrane permeable (Zhu et al., 1998). We show that dye fluxes are much larger—by as much as an order of magnitude—as compared with fluxes measured in nonmeristematic cells, and we validate the protocol by confirming that dye fluxes are decreased in transgenic lines with known impairment in plasmodesmal function. Furthermore, we assay several chemical treatments that might regulate plasmodesmal gating: the aromatic amino acid, Trp; the growth regulator, auxin; and the reactive oxygen species, hydrogen peroxide (H_2O_2).

RESULTS

Plasmodesmal Permeability from Tissue-Scale Analysis

We loaded dye into the cells of the meristem by incubating the roots of intact seedlings in the diacetate derivative of CF for 7 min. The seedlings were then transferred to dye-free growth medium and moved to the stage of a confocal fluorescence microscope for photobleaching and recovery. The observed recovery of fluorescence intensity is used to obtain an effective diffusion constant D and an effective permeability P, as outlined below.

Photobleaching single cells was challenging because of the rapidity of dye recovery and the difficulty of deriving an accurate permeability value from the bleaching geometry of cells in the root. Although we do use a single-cell method for verification (see "Plasmodesmal Permeability from Cell-Scale Analysis" below), we found that a more robust and reproducible method for obtaining a diffusion coefficient was by photobleaching dye in a large block of cells. The root is bleached in a 50-μm-long zone (approximately six cell lengths), spanning the width of the root and located about 200 μm from the quiescent center (Fig. 1). The bleach penetrated all visible layers of the root, not just the epidermis, and retained a length of approximately 50 μm at all depths (Supplemental Fig. S1). Image intensity was averaged across the width of the root, which allowed us to approximate fluorescence recovery as a diffusion problem in one dimension. The diffusion coefficient we measured in this way com-

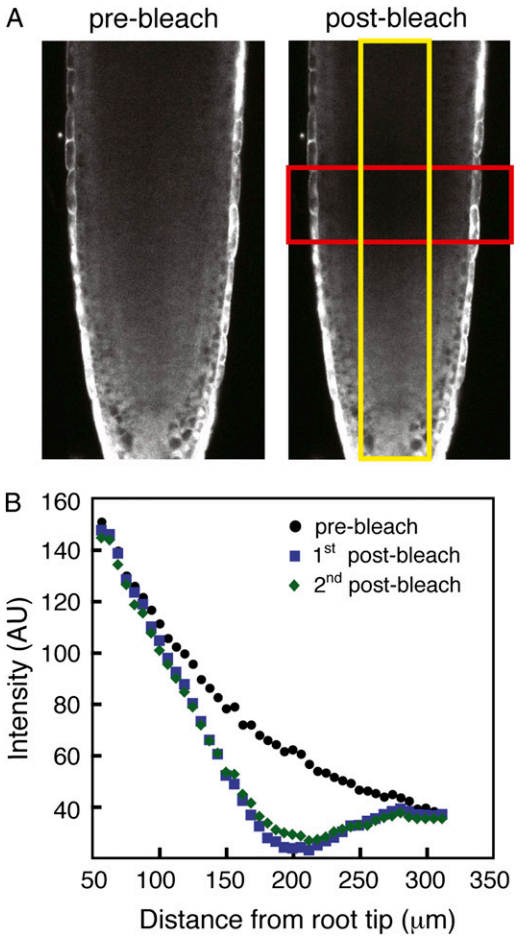

Figure 1. Tissue-scale analysis of plasmodesmal permeability in the root meristem. A, The region marked by the red box is bleached for about 30 s. Recovery images are cropped (yellow box) to exclude the edges of the root, and intensity is averaged perpendicular to the root's long axis. This produces a one-dimensional intensity profile, used for analysis. B, The intensity profile (arbitrary units [AU]) before the bleach (black), at 4 s after the bleach (blue), and at 13.3 s after the bleach (green). The difference between blue and green data sets is plotted in Figure 2.

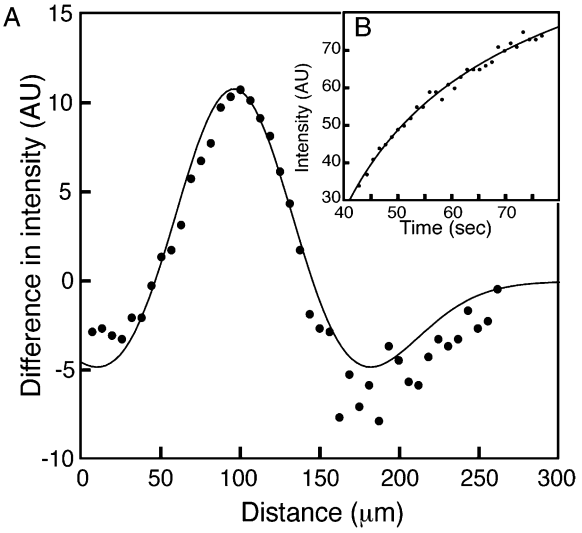

Figure 2. The model used to quantify diffusion. A, Symbols plot the difference in intensity between two post-bleach intervals. The solid line plots Equation 3 fitted to these data. Note that the central zone gets brighter while adjacent zones get dimmer during recovery, showing that longitudinal diffusion is carrying unbleached dye into the bleach zone. B, Data used to obtain the parameter t_o. Symbols plot intensity versus time for the darkest part of the bleach. Solid line plots Equation 2 fitted to these data.

bined the effects of diffusion within the cytoplasm and transport through plasmodesmata, so we refer to it as an effective diffusion coefficient.

To find the effective diffusion coefficient, we compared the recovery data with an approximate mathematical model of the experiment. Following photobleaching, the intensity profile $I(x,t)$ is well described by the steady-state solution, $I_{ss}(x)$, minus a diffusing mass of bleached dye with a Gaussian profile, as:

$$I(x,t) = I_{SS}(x) - \frac{B}{\sqrt{t-t_0}}\exp\left(\frac{-(x-x_0)^2}{4D(t-t_0)}\right) \quad (1)$$

where I_{SS} is the steady-state intensity that would be achieved if diffusion ran to completion, and the rightmost term is the solution to the diffusion equation on an infinite line with an initially Gaussian distribution. The constant B characterizes the depth of the bleach, x_0 is the location of the center of the bleach, t_0 is the effective starting time, and D is the effective diffusion coefficient.

We first found a preliminary location for the center of the bleach, x'_0, using a parabolic curve fit to $I(x)$ at early post-bleach times. Then, to find t_0, the intensity at the center of the bleach is fit to Equation 1 with $x = x'_0$, namely:

$$I(x'_0,t) = I_{SS}(x'_0) - \frac{B}{\sqrt{t-t_0}} \quad (2)$$

To eliminate the unknown function $I_{SS}(x)$ from our analysis, we subtracted intensity data at two consecutive times, t_1 and t_2, and fit the difference to:

$$F(x,t_1,t_2) = I(x,t_2) - I(x,t_1) = \frac{B}{\sqrt{t_1-t_0}}\exp\left(\frac{-(x-x_0)^2}{4D(t_1-t_0)}\right) - \frac{B}{\sqrt{t_2-t_0}}\exp\left(\frac{-(x-x_0)^2}{4D(t_2-t_0)}\right) \quad (3)$$

where t_0 is obtained as described above, and t_1 and t_2 are known from the image acquisition times. Best results are achieved when the intensities vary rapidly, so we generally chose times within 15 s from the end of the bleach. In cases where the diffusion was relatively slow (specifically, for high concentrations of H_2O_2), we averaged over longer times. The curve fit to Equation 3 yields values for B, D, and an improved value for the bleach center, x_0. The value for x_0 is used to validate the original choice for the intensity minimum, and D is the desired diffusion coefficient. Using this approach, values for an effective diffusion constant were recovered with good reproducibility (see below).

Having found the effective diffusion coefficient, D, we can convert this to a plasmodesma-mediated wall permeability, P. In general, the flux of a solute diffusing through the plasmodesmata is given by:

$$J = P(c_1 - c_2) \quad (4)$$

where J is the flux (moles crossing a unit area of wall per unit time) from cell 1 to 2, c_1 and c_2 are the solute concentrations adjacent to the open ends of the plasmodesmata, and P is a diffusive permeability, which will depend on the solute under consideration. Since our protocol does not resolve the concentration at the walls, we instead tracked the average solute concentration of an entire cell. In this case, the appropriate version of Fick's law is:

$$J = D\left(\frac{C_2 - C_1}{L}\right) \quad (5)$$

where C_1 and C_2 are the average concentration in cell 1 and 2, L is the mean cell length, and D is our effective diffusion coefficient.

As mentioned above, our value for D incorporates the effects of both the plasmodesmal permeability and the diffusion of solute within the cytoplasm. The relationship between P and D can be calculated for a single file of cells as:

$$P = \frac{D/L}{1 - D/D_{cyt}} \quad (6)$$

where L is the mean cell length, and D_{cyt} is the diffusion coefficient of dye in the cytoplasm. The numerator (D/L) is the permeability estimate in the case where the cytoplasm is well mixed, and the denominator is a correction due to the cytoplasmic dye gradient that accompanies diffusion (Kramer, 2002). Thus, a value for permeability can be obtained from the effective diffusion constant for the bulk tissue (measured above), the mean cell length in the region, and the cytoplasmic diffusion constant. For mean cell length, we measured the average length of cortex cells in the region used for bleaching (see Table III). In some experiments below,

treatments lasted only 2 h, and for those we used the control (wild type) cell length because meristematic cell growth is approximately 5% h^{-1} (Beemster and Baskin, 1998) and hence can undergo little change within that interval. Our value obtained for the wild type agrees with previous results (Beemster and Baskin, 1998). We take the diffusion constant for CF in the cytoplasm, D_{cyt}, as 162 $\mu m^{-2}\ s^{-1}$, which is one-third of its aqueous value (Paine et al., 1975; Kramer et al., 2007). The permeability thus obtained (see Fig. 4B) is almost an order of magnitude greater than previous reports (Goodwin et al., 1990).

Plasmodesmal Permeability from Cell-Scale Analysis

To validate the results from tissue-scale photobleaching, we developed an alternative method based on photobleaching single cells. Single-cell bleaches were challenging because dye moved rapidly between cells (<1 s), and because dye movement in three dimensions was difficult to model. We achieved satisfactory single-cell results for epidermal cells only. To minimize photobleaching of adjacent cells, the bleaching region was limited to a circular spot, approximately 10 μm^2 and centered within the target cell. Since the vacuole was relatively dark, by necessity the bleaching region overlay the nucleus. The nucleus is in diffusive communication with the cytoplasm, and bleached dye moved quickly (<1 s) between compartments.

Rather than monitoring brightness recovery, we measured intensity during the bleaching process itself. We built a time course by taking the first post-bleach frame from a series of progressively longer bleaches (Fig. 3), effectively tracking the rate of brightness loss. In Supplemental Information S1, we derive the following equation for the rate of change of intensity of a bleached nucleus during an ongoing bleach

$$\frac{dn_1}{dt} = \left(\frac{PA}{V}\right)(n_2 - n_1) - \frac{n_1}{\tau} - b \qquad (7)$$

where n_1 and n_2 are the intensities of the bleached nucleus and an adjacent nucleus, respectively, P is the cell wall permeability between epidermal cells, A is the cell wall area, V is the volume of the cell, τ is a time scale characterizing the strength of the bleach, and b is a constant. The first term on the right represents the diffusive movement of dye from the adjacent unbleached cells into the bleached cell, the second term represents the loss of dye due to bleaching, and the constant term b is an approximate correction to allow for the fact that the nuclear brightness will in general be different from the cytoplasmic brightness.

With measurements of n_1, n_2, and dn_1/dt, we find the coefficients in Equation 7 using linear regression. This gives values for τ, b, and the ratio PA/V. The wall area A, and cell volume V, are measured from a corresponding z stack of the bleached cell. We found the resulting value for plasmodesmal permeability of a single epidermal cell wall to be $P = 3.3 \pm 0.8\ \mu m\ s^{-1}$ (SEM, $n = 4$). This is approximately half that obtained from the tissue-scale bleach protocol. Insofar as the single-cell analysis involves the epidermis and the tissue-scale analysis involves multiple cell layers, their agreement within a factor of two gives us confidence in these measurements of permeability.

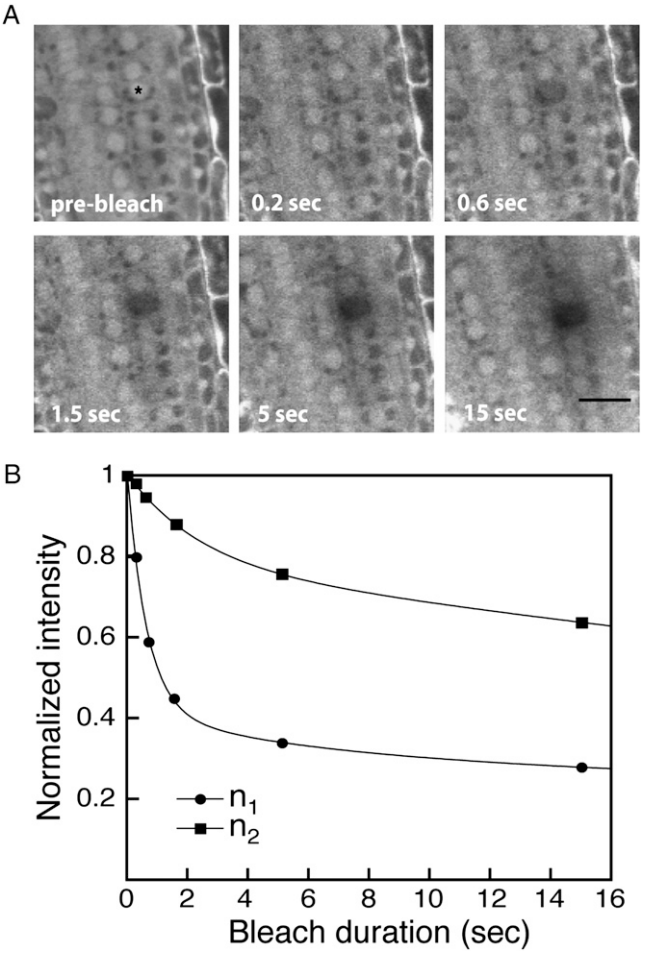

Figure 3. Single-cell analysis. A, Images illustrating the method. A region of interest about 10 μm^2 (asterisk in frame 1), within a single epidermal cell, is bleached for the amount of time shown and an image acquired immediately afterward. The time between bleaches, approximately 2 min, is sufficient to allow essentially complete recovery. Concatenated, the images approximate the progress of a single bleach. Bar = 20 μm. B, Intensity versus time for a single-cell bleach. Symbols are data, solid lines are a guide to the eye. Note rapid bleaching within the target nucleus (n_1) and the more gradual spread of bleached dye to the adjacent nucleus (n_2). For each nucleus, intensity is normalized to the prebleach value.

Analysis of Lines with Reduced Plasmodesmal Conductivity

To validate further our measurements of diffusion and resulting permeability, we applied the bulk bleaching protocol to plant lines where plasmodes-

mata are reported to be perturbed. First, we tested an Arabidopsis line overexpressing PLASMODESMATA CALLOSE BINDING1 (PDCB1; Simpson et al., 2009). Endogenous PDCB1 binds callose and localizes to the apoplast around plasmodesmata. In the overexpression line *35S::YFP-PDCB1*, cytosolic GFP introduced into leaf epidermal cells by bombardment undergoes reduced cell-to-cell movement as compared with wild type. We find that permeability in this line was about one-half that of wild type (Fig. 4).

Second, we assayed permeability in *radially swollen6* (*rsw6*), a line isolated on the basis of temperature-dependent root swelling and reported to have defective organization of cortical microtubules (Bannigan et al., 2006). The roots of *rsw6* are similar to wild type at temperatures below about 22°C and express the root swelling phenotype at higher temperatures. Following incubation of *rsw6* at 30°C for 6 h, dye movement in the epidermis and cortex is qualitatively reduced compared to wild type (Bannigan, 2003). Consistent with these observations we measured a substantial decrease in permeability for *rsw6* under the same conditions (Fig. 4). Thus, in two distinct genetic backgrounds, our assay quantifies a reduced plasmodesmal permeability consistent with previous, qualitative reports.

Alteration of Plasmodesmal Permeability

Having established a means to quantify plasmodesmal permeability, we used it to probe several situations where permeability might be expected to change. In an earlier study of *Egeria densa* leaves, microinjection of various aromatic amino acids at 10 mM significantly reduced plasmodesmal permeability to small molecules, implying a level of specific regulation (Erwee and Goodwin, 1984). Therefore, we first assayed the effects of the aromatic amino acid, Trp. To determine relevant concentrations, we transferred untreated seedlings to plates containing Trp and measured root elongation rate over the next three days (Fig. 5A). On 0.3-mM Trp, root elongation rate did not differ significantly from the control but on 0.4 mM, elongation rate decreased to below 20% of the control. Thus, for permeability assays, we chose 0.3 mM as a low concentration of Trp, and 0.6 mM as a high value.

For tissue-scale permeability assays, 6-d-old seedlings were transferred to plates containing the indicated concentration and assayed after 2 h (Table I) and after 24 h of treatment (Table II). At either time, the low concentration (0.3 mM) had no significant effect on permeability. The high concentration (0.6 mM) reduced permeability at 24 h by about 30%; and at 2 h, permeability tended to be decreased although the effect was not significant.

We next assayed the effect of the plant hormone auxin (indoleacetic acid [IAA]). We chose a low concentration of 30 nM IAA, which inhibits root elongation rate by approximately 50%, and a high concentration of 100 nM IAA, which stops growth almost completely

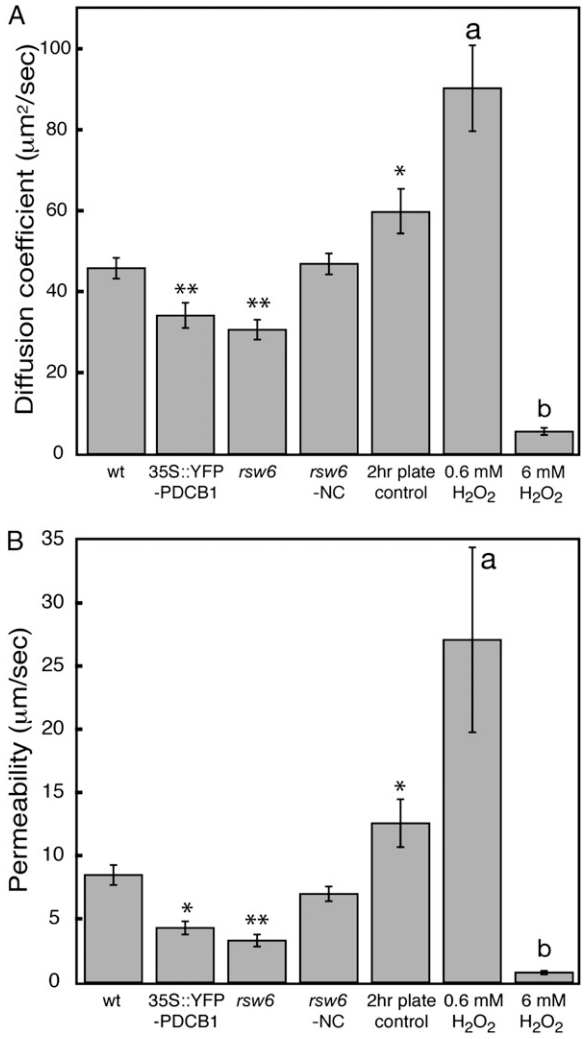

Figure 4. Tissue-scale analysis. A, Effective diffusion coefficients. B, Plasmodesmal permeabilities. The *rsw6* line was either exposed to the restrictive temperature for 6 h (*rsw6*) or maintained at the permissive temperature (*rsw6*-NC). The cell lengths used to calculate permeability are shown in Table III; for the 2-h treatments, the wild-type cell length was used. For treatment with H_2O_2, wild-type seedlings were grown for 7 d, then transferred to agar plates containing growth medium alone (2-h plate control) or with H_2O_2 for 2 h before assay. $n \geq 17$ for all treatments. Equivalence of means between wild type and mutants or 2-h plate control rejected at (*) $P < 0.05$ or (**) $P < 0.01$; equivalence of means between 2-h plate control and peroxide treatments rejected at $P < 0.05$ (a) or $P < 0.001$ (b).

(Rahman et al., 2007). After 2 h of treatment, permeability did not significantly differ from the control on either concentration (Table I). We also assayed roots after treatment with 30 nM IAA for 24 h and again, permeability did not significantly differ from control (Table II). We did not assay a 24-h treatment with 100 nM IAA because the complete inhibition of growth seems nonphysiological. These results suggest that flux through plasmodesmata is generally insensitive to increasing auxin levels.

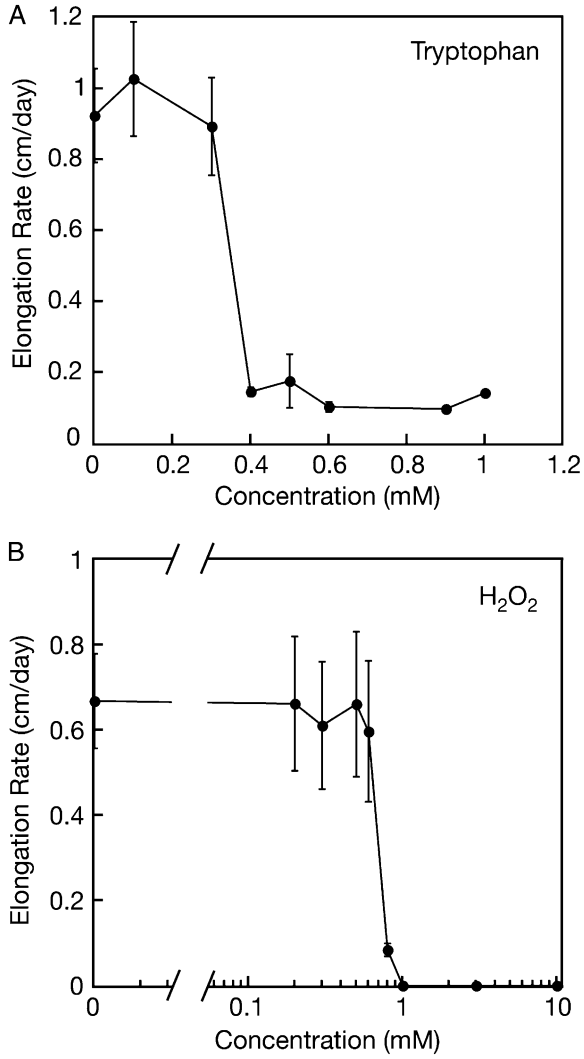

Figure 5. Root elongation rate as a function of concentration for Trp (A) and H_2O_2 (B). Four-day-old wild-type seedlings were transferred to media containing the indicated concentrations and the root elongation rate measured at daily intervals over the next 3 d. Symbols plot the mean daily growth rate ± SEM (when larger than the symbol) of three replicate experiments.

For the controls in Tables I and II, permeability for the 2-h treatment was higher than that of the 24-h treatment and the difference was significant (see Fig. 4). For treatments, seedlings are transferred from one (control) plate to another (treatment) plate. Although lasting only a few minutes per treatment, transfer involves exposure to air, horizontal placement, and mechanical stress, any of which might have led to an increase in plasmodesmal flux. By 24 h, this effect had apparently subsided, in that recorded permeability values matched those of seedlings never transferred between plates. That this relatively mild transfer treatment significantly altered flux through plasmodesmata underscores the sensitivity of our assay.

Curiously, the production of reactive oxygen species has been associated with both an increase (Benitez-Alfonso et al., 2009) and a decrease (Stonebloom et al., 2009) in the size exclusion limit of plasmodesmata. To determine to what extent reactive oxygen affects plasmodesmal solute flux, we assayed the effects of treatment with H_2O_2, a typical reactive oxygen species. To select relevant concentrations, we assayed root elongation rate (Fig. 5B). Root elongation rate was similar to controls on 0.6 mM H_2O_2, but was reduced to negligible levels on 1 mM H_2O_2. We chose 0.6 mM H_2O_2 as the low concentration, and 6 mM as the high concentration. To assay plasmodesmal permeability, we transferred 7-d-old seedlings to treatment plates for 2 h. Strikingly, treatment with the low concentration of H_2O_2 increased plasmodesmal permeability by factor of two, whereas the high concentration nearly abolished it (Fig. 4).

To our knowledge, these results are the first reported quantitative changes in solute flux through plasmodesmata on a 2-h time scale. This implies an active regulation of symplastic connectivity.

DISCUSSION

The observed plasmodesmal fluxes between cells of the Arabidopsis root meristem are unexpectedly rapid. In fact, in our initial attempts to monitor the fluorescence recovery of single bleached cells, we acquired images at one frame per 5 s and missed the recovery process entirely. This is one reason we turned instead to a protocol in which a large volume of the root meristem is bleached. The large cytoplasmic volume slows down the time scale of diffusive recovery, and the involvement of hundreds of cells reduces the impact of cell-to-cell heterogeneity. Our results indicate that adjacent meristem cells will equilibrate small solutes in just a few seconds.

Although our results rely principally on tissue-scale bleaches, we did perform some single-cell bleaches for

Table I. *Effective diffusion constants and permeabilities for Arabidopsis roots treated with Trp or auxin for 2 h*

Tissue-scale analysis, with 7-d-old seedlings treated as indicated for 2 h. Data are mean ± SEM, with $n \geq 17$ for *D*. To calculate *P*, the average cell length for the control was used for all treatments. For *P*, errors were propagated as described in "Materials and Methods." The control data are for a 2-h transplant onto fresh growth medium (same data shown in Fig. 4, A and B). For either *D* or *P*, no statistical support was found for rejecting the equivalence of control and experimental means.

Treatment	*D*	*P*
	$\mu m^2\ s^{-1}$	
Control	59.9 ± 5.4	12.6 ± 1.9
Trp (0.3 mM)	57.6 ± 5.3	11.8 ± 1.8
Trp (0.6 mM)	47.4 ± 4.9	8.9 ± 1.4
IAA (30 nM)	50.7 ± 5.1	9.8 ± 1.5
IAA (100 nM)	60.5 ± 6.5	12.8 ± 2.3

Table II. *Effective diffusion constants and permeabilities for Arabidopsis roots treated with Trp or auxin for 24 h*

Tissue-scale analysis, with 6-d-old seedlings treated as indicated for 24 h. Data are mean ± sem, with n ≥ 17 for D. For P, errors are propagated as described in "Materials and Methods." Average cortical cell length was measured for each treatment after 24 h and used in the calculation of P (the cell lengths are shown in Table III). Control data are for undisturbed seedlings (same data shown in Fig. 4, A and B).

Treatment	*D*	*P*
	$\mu m^2\ s^{-1}$	$\mu m\ s^{-1}$
Control	45.9 ± 2.6	8.5 ± 0.8
Trp (0.3 mM)	45.4 ± 4.9	6.4 ± 1.2
Trp (0.6 mM)	32.0 ± 4.3[a]	4.6 ± 0.9[a]
IAA (30 nM)	37.5 ± 8.6	6.0 ± 1.8

[a]Equivalence to the control mean rejected at $P < 0.05$ by *t* test.

validation purposes. The permeability value measured for the transverse walls of single epidermal cells (3.3 μm s^{-1}) is 2- to 3-times smaller than values measured in the tissue as a whole (6 to 8.5 μm s^{-1}). Since the intensity data collected for single cells are for epidermis whereas those for the tissue-scale analysis are dominated by the large cross-sectional area of cortical cells, the difference could reflect a difference in permeability between epidermis and cortex. Indeed, in the Arabidopsis root meristem, plasmodesmal frequency in transverse walls of cortical cells is about twice as high as that in the epidermis (Zhu et al., 1998), a finding that plausibly accounts for the 2-fold difference we report for permeability.

To our knowledge, plasmodesmal permeability has been reported explicitly in only one previous article (Goodwin et al., 1990). These authors tracked the movement of dye microinjected into leaf epidermal cells of *E. densa* and reported a permeability of 1.1 μm s^{-1} for CF, and 10 times less for fluorescein conjugated to single amino acids. Our bulk permeability values for the Arabidopsis meristem are nearly an order of magnitude larger. We suggest that the difference is due in part to the noninvasive nature of our method, whereby a puncture-wound response was avoided. The difference could also reflect programmed permeability decreases coincident with differentiation, as previously observed using CF in roots (Duckett et al., 1994) and GFP in embryos (Kim and Zambryski, 2005).

Although obtained for fairly unusual tissues such as aquatic leaves or stamen hairs, earlier measurements of dye permeability and diffusion have been influential whenever a value for the transport capacity of the symplast has been needed. For example, Bret-Harte and Silk (1994) used results from a study of diffusion in stamen hairs (Tucker et al., 1989) to infer that the symplasmic pathway in the maize (*Zea mays*) root apex cannot transport enough Suc to sustain measured rates of dry mass deposition. However, with the permeability values reported here, symplastic transport would be sufficient.

Our assay also revealed that H_2O_2 increases or decreases plasmodesmal flux based on concentration (Fig. 4, A and B). This biphasic regulation is suggestive of two recent reports that have implicated reactive oxygen species in the regulation of plasmodesmal function, but in a contradictory way. Both reports featured Arabidopsis loss-of-function mutants. The first mutation is *increased size exclusion1* (*ise1*), which occurs in a mitochondrial RNA helicase (Stonebloom et al., 2009), and the other is *GFP arrested trafficking1* (*gat1*), which occurs in an m-type, plastid-localized thioredoxin (Benitez-Alfonso et al., 2009). In both mutants, roots accumulate reactive oxygen species; however, the symplastic permeability phenotypes are opposite, increasing in *ise1* and decreasing in *gat1*. Based on our results, we hypothesize that the opposite permeability phenotypes of the two mutants is explained by the degree to which reactive oxygen species accumulate, with a large increase in *gat1* and a small increase in *ise1*.

Also consistent with our results, Benabdellah et al. (2009) found in *Phaseolus vulgaris* roots that H_2O_2 exerts biphasic effects on bulk hydraulic conductivity, increasing it at low concentrations (below about 1 mM) and decreasing it at higher concentrations. Although their results did not distinguish contributions from symplastic and apoplastic pathways, taken together with ours, it suggests that the movement of small molecules including water is generally promoted by modest increase of reactive oxygen species and restricted by a larger increase. A speculative explanation for this response is that low levels of peroxide signal a state of stress that can be ameliorated by increased exchange of water and nutrients, while higher levels signal a dangerous state, such as pathogen invasion, where cell isolation is beneficial.

We also tested the effects of several other exogenous chemical treatments on plasmodesmal permeability. The aromatic amino acid, Trp, slows dye movement significantly at 0.6 mM after 24 h, consistent with earlier qualitative work (Erwee and Goodwin, 1984). Since Trp concentration in plant tissues is between 0.1 and 1 mM (Soudry et al., 2005), these observations might indicate a role for Trp in the regulation of plasmodesmal flux.

Trp is an aromatic indole compound like the hormone IAA, and is also one of its biosynthetic precursors (Normanly, 2010). Despite the efficacy of the related compound Trp, IAA itself does not regulate plasmodesmatal permeability at physiologically relevant levels, both at 2- and 24-h treatment times.

Since auxin does not gate plasmodesmata, we wondered whether the large permeabilities reported here would allow auxin to cross cell walls fast enough to short circuit polar auxin transport. In fact, the permeabilities measured here are still consistent with auxin transport, according to a straightforward mathematical argument. In the simplest model of polar auxin transport, one considers a single, uniform file of nonvacuolated cells. The equation for the speed of auxin transport, *v*, through this cell file is

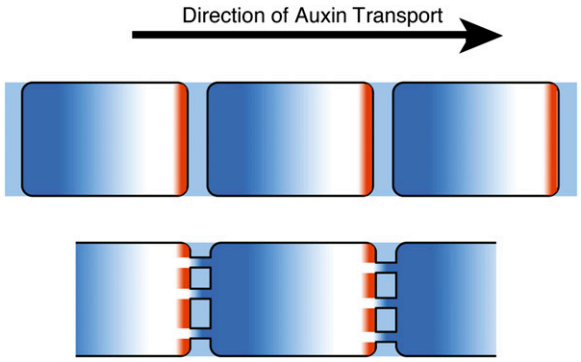

Figure 6. Sketch of auxin levels in a file of auxin-transporting cells. Blue: auxin concentration; red: PIN-family efflux carriers. Note that the cytoplasmic auxin is depleted near the efflux carriers. Top, A file with no open plasmodesmata; bottom, the addition of open plasmodesmata provide a diffusive pathway in the wrong direction.

$$v = \frac{p}{1 + (p/2 + q)(L/D_{cyt})} \quad (8)$$

where D_{cyt} is the cytoplasmic diffusion coefficient of auxin, L is the cell length, p is the contribution to the cell wall permeability from the polar distribution of PIN carriers, and q is the contribution to cell wall permeability from any nonpolar auxin carriers as well as from open plasmodesmata (Mitchison, 1980; Kramer, 2002).

To assess the impact of open plasmodesmata on auxin transport, we need to assign approximate values to the variables in Equation 8. The PIN permeability will be approximately equal to the auxin transport speed, which in most tissues is about 1 cm h^{-1} (Kramer, 2004), so we set P = 1 cm h^{-1} = 2.8 μm s^{-1}. The cytoplasmic diffusion coefficient of auxin is perhaps one-third of its aqueous value, D_{cyt} = 220 μm^2 s^{-1} (Paine et al., 1975). Assuming that open plasmodesmata make the largest contribution to q, we can use a typical permeability reported here, q = 10 μm s^{-1}. For a file of cells 10 μm in length, Equation 8 gives $v = p/1.5$ = 1.8 μm s^{-1}, a reduction below p of 34%; however, for a file of 100-μm long cells, we have $v = p/6.1$ = 0.45 μm s^{-1}, a reduction below p by 84%. Therefore, the plasmodesmal permeability can be several times larger than the PIN permeability and still cause only a modest reduction of auxin transport speed, at least for smaller cells.

Competition between plasmodesmata and PIN proteins is made explicit in Equation 8 through the dimensionless quantity $q(L/D_{cyt})$. To see the importance of this quantity, recall that polar auxin transport is believed to rely on diffusion to move auxin within the cell. Thus, one expects a maximum in the cytoplasmic auxin concentration at the upstream end of the cell and an auxin minimum adjacent to the PIN efflux proteins (Fig. 6). The ratio, D_{cyt}/L, characterizes the diffusion of auxin through the cytoplasm from the auxin maximum to the auxin minimum (the forward flux) while the permeability q characterizes the flux of auxin through the cell wall back to the previous minimum (the backward flux). The ratio of reverse to forward fluxes is thus $q(L/D_{cyt})$. This ratio is 0.45 for a file of 10-μm cells and 4.5 for 100-μm cells. This might be one reason why cell enlargement coincides with a gradual restriction of flux through plasmodesmata, because otherwise polar auxin transport would be impractical in elongated cells.

Our method for quantifying plasmodesmal flux takes advantage of the small size, relative transparency, and lack of autofluorescent chlorophyll in the Arabidopsis root, features that allow for easy dye loading and manipulation. However, the method could be applied to other tissues with appropriate modifications. It should also be straightforward to use this technique with larger fluorescent molecules and proteins, and thereby quantify plasmodesmal permeability for probes of different sizes and structure. Care must be taken to ensure that the rates of probe synthesis and degradation are low compared to the time scale of diffusion through the plasmodesmata; these requirements are met for ester-loaded CF in the root meristem. Using this method, we have characterized a rapid and flexible regulation of plasmodesmal permeability in the Arabidopsis root meristem. Understanding how plasmodesmata are gated now becomes an important goal for future research.

MATERIALS AND METHODS

Plant Growth and Treatments

Arabidopsis (*Arabidopsis thaliana*) seeds were surface sterilized, rinsed, and planted on agar plates containing 1% Bacto-agar (Difco) and 1% Suc in a modified Hoagland medium placed vertically in constant, yellow light (approximately 100 μmol $m^{-2}s^{-1}$) at 22°C, as described previously (Bannigan et al., 2006). All material was in the Columbia background. For experimental treatments, seedlings were grown for 5 to 7 d before transfer to fresh agar plates containing the compound of interest and then returned to the growth chamber for the indicated interval (usually between 2 and 24 h). For H_2O_2, agar plates were prepared with the required concentration 1 h prior to transfer to ensure maximum activity of the compound. Assays of root elongation rate were done as described previously (Rahman et al., 2007).

Table III. *Average cortical cell length used for tissue-scale analysis*

For wild type, *35S::YFP-PDCB1*, and *rsw6*, 7-d-old seedlings were measured. For Trp and auxin, measurements were taken after 6-d-old seedlings were treated as indicated for 24 h. Data are mean ± SEM, with $n \geq 44$ individual cells and at least three roots per genotype or treatment.

Genotype/Treatment	Cell Length
	μm
Wild type	7.5 ± 0.4
35S::YFP-PDCB1	9.4 ± 0.5[a]
rsw6	11.2 ± 0.7[a]
rsw6-NC	9.4 ± 0.4[a]
Trp (0.3 mM)	9.7 ± 0.5[a]
Trp (0.6 mM)	8.3 ± 0.6
IAA (30 nM)	8.2 ± 0.3

[a]Equivalence to the control mean rejected at $P < 0.01$ by t test.

Dye Loading and Confocal Microscopy

Whole seedlings were removed from agar plates and roots were incubated in 30 mg/mL carboxyfluorescein diacetate in growth medium for 7 min. Excess dye solution was removed with tissue paper. To avoid CF being generated during recovery from photobleaching, the root was rinsed once with growth medium, and then surrounded by fresh growth medium for imaging. A coverslip was applied to reduce movement during imaging, and the root was immediately imaged on a confocal fluorescence microscope (either a Nikon Eclipse TE-2000S or a Zeiss LSM 510) with a 40× objective. Tissue-scale diffusion was measured by bleaching a 50-μm-long segment of the root meristem, approximately 200 μm behind the quiescent center, for 35 to 40 s. The focal plane is centered within the root cortex, as optical sections closer to the stele are too dim to monitor. The confocal pinhole is opened to give a focal depth of about 10 μm. Setting a thick focal plane allows us to reduce the laser intensity and thereby limit bleaching affects. Also, averaging over a thicker volume reduces the effects of micron-scale fluctuations in brightness. The image acquisition rate during brightness recovery was typically one frame per 1.5 s, which includes an exposure time of 0.7 to 0.8 s per image. The mathematical details of the analysis used to determine the diffusion coefficient D and the wall permeability P are described in the main text.

To image the geometry of the bleach during measurements of tissue-scale diffusion, we first treated a wild-type root with 6 mM H_2O_2 for 2 h, sufficient to reduce plasmodesmal permeability to negligible levels (Fig. 4, A and B). The root was then placed on the confocal as described above and subjected to a 35 to 40 s bleach. We collected a z stack of the meristem immediately following the bleach and used ImageJ (v1.38x, http://rsbweb.nih.gov/ij/) to project an image of the x-z plane (Supplemental Fig. S1).

For single-cell bleaches, the roots were loaded with CF and imaged with the confocal as above. Procedural details of the bleaches used to measure permeability are provided in the main text, and further mathematical analysis is described in the Supplemental Information S1 and Supplemental Figure S2.

To measure cell length, 7-d-old roots were immersed in 1.0 μM FM4-64 for 5 min to stain the cell membranes. Roots were rinsed in growth medium and then imaged on a Nikon Eclipse TE-2000S confocal microscope with a 40× objective. All cell length measurements were made in the same region as used for bleaching. The values of average cell length used to convert the effective diffusion constant to a permeability (according to Eq. 6) are given in Table III.

Data Analysis

Images were analyzed using ImageJ and curve fits were performed using KaleidaGraph (v3.6.4; Synergy Software). For tissue-scale analysis, several frames were averaged and the midpoint time taken as t_n. SES for the permeability shown here (Tables I and II; Fig. 4) were calculated using the general formula for propagation of errors in Sec 4-1 of Bevington (1969), assuming zero covariance between D and L. In the case of a t test for statistically significant differences between pairs of P values, we made a conservative estimate for the degrees of freedom using (d.o.f. P) = min (N_D, N_L) − 2, where N_L is the number of roots used to determine cell length and N_D is the number of measurements made for D.

Supplemental Data

The following materials are available in the online version of this article.

Supplemental Figure S1. Profile of a transverse bleach.

Supplemental Figure S2. Sketch of the geometry for a single-cell analysis.

Supplemental Information S1. Derivation of Equation 5 for plasmodesmal permeability from a single-cell analysis.

ACKNOWLEDGMENTS

We thank Dr. Andrew Maule (John Innes Center, Norwich, UK) for the generous gift of the *35S::YFP-PDCB1* line.

Received October 26, 2010; accepted February 10, 2011; published February 16, 2011.

LITERATURE CITED

Bannigan A (2003) The relationship between intercellular communication and microtubule organization in plants. PhD thesis. University of Sydney, Sydney

Bannigan A, Wiedemeier AMD, Williamson RE, Overall RL, Baskin TI (2006) Cortical microtubule arrays lose uniform alignment between cells and are oryzalin resistant in the Arabidopsis mutant, radially swollen 6. Plant Cell Physiol **47:** 949–958

Beemster GTS, Baskin TI (1998) Analysis of cell division and elongation underlying the developmental acceleration of root growth in *Arabidopsis thaliana*. Plant Physiol **116:** 1515–1526

Benabdellah K, Ruiz-Lozano JM, Aroca R (2009) Hydrogen peroxide effects on root hydraulic properties and plasma membrane aquaporin regulation in *Phaseolus vulgaris*. Plant Mol Biol **70:** 647–661

Benitez-Alfonso Y, Cilia M, San Roman A, Thomas C, Maule A, Hearn S, Jackson D (2009) Control of Arabidopsis meristem development by thioredoxin-dependent regulation of intercellular transport. Proc Natl Acad Sci USA **106:** 3615–3620

Bevington PR (1969) Data Reduction and Error Analysis for the Physical Sciences. McGraw-Hill, New York, pp 56–65

Bret-Harte MS, Silk WK (1994) Nonvascular, symplasmic diffusion of sucrose cannot satisfy the carbon demands of growth in the primary root tip of *Zea mays* L. Plant Physiol **105:** 19–33

Duckett CM, Oparka KJ, Prior DAM, Dolan L, Roberts K (1994) Dye-coupling in the root epidermis of Arabidopsis is progressively reduced during development. Development **120:** 3247–3255

Erwee MG, Goodwin PB (1984) Characterization of the *Egeria densa* leaf symplast: response to plasmolysis, deplasmolysis and to aromatic amino acids. Protoplasma **122:** 162–168

Erwee MG, Goodwin PB (1985) Symplast domains in extrastellar tissues of *Egeria densa* Planch. Planta **163:** 9–19

Goodwin PB, Shepherd V, Erwee MG (1990) Compartmentation of fluorescent tracers injected into the epidermal cells of *Egeria densa* leaves. Planta **181:** 129–136

Kim I, Zambryski PC (2005) Cell-to-cell communication via plasmodesmata during Arabidopsis embryogenesis. Curr Opin Plant Biol **8:** 593–599

Kramer EM (2002) A mathematical model of pattern formation in the vascular cambium of trees. J Theor Biol **216:** 147–158

Kramer EM (2004) PIN and AUX/LAX proteins: their role in auxin accumulation. Trends Plant Sci **9:** 578–582

Kramer EM, Frazer NL, Baskin TI (2007) Measurement of diffusion within the cell wall in living roots of Arabidopsis thaliana. J Exp Bot **58:** 3005–3015

Lucas WJ, Bouché-Pillon S, Jackson DP, Nguyen L, Baker L, Ding B, Hake S (1995) Selective trafficking of KNOTTED1 homeodomain protein and its mRNA through plasmodesmata. Science **270:** 1980–1983

Maule AJ (2008) Plasmodesmata: structure, function and biogenesis. Curr Opin Plant Biol **11:** 680–686

Mitchison GJ (1980) The dynamics of auxin transport. Proc R Soc Lond B Biol Sci **209:** 489–511

Nakajima K, Sena G, Nawy T, Benfey PN (2001) Intercellular movement of the putative transcription factor SHR in root patterning. Nature **413:** 307–311

Normanly J (2010) Approaching cellular and molecular resolution of auxin biosynthesis and metabolism. Cold Spring Harb Perspect Biol **2:** a001594

Oparka K, Duckett C, Prior D, Fisher D (1994) Real-time imaging of phloem unloading in the root tip of *Arabidopsis*. Plant J **6:** 759–766

Paine PL, Moore LC, Horowitz SB (1975) Nuclear envelope permeability. Nature **254:** 109–114

Radford JE, White RG (2001) Effects of tissue-preparation-induced callose synthesis on estimates of plasmodesma size exclusion limits. Protoplasma **216:** 47–55

Rahman A, Bannigan A, Sulaman W, Pechter P, Blancaflor EB, Baskin TI (2007) Auxin, actin and growth of the Arabidopsis thaliana primary root. Plant J **50:** 514–528

Rinne PLH, van der Schoot C (1998) Symplasmic fields in the tunica of the shoot apical meristem coordinate morphogenetic events. Development **125:** 1477–1485

Robards AW, Lucas WJ (1990) Plasmodesmata. Annu Rev Plant Physiol Plant Mol Biol **41:** 369–419

Schulz A (1999) Physiological control of plasmodesmal gating. *In* WJP

AavK van Bel, ed, Plasmodesmata: Structure, Function, Role in Cell Communication. Springer, Berlin, pp 173–204

Simpson C, Thomas C, Findlay K, Bayer E, Maule AJ (2009) An *Arabidopsis* GPI-anchor plasmodesmal neck protein with callose binding activity and potential to regulate cell-to-cell trafficking. Plant Cell **21:** 581–594

Soudry E, Ulitzur S, Gepstein S (2005) Accumulation and remobilization of amino acids during senescence of detached and attached leaves: in planta analysis of tryptophan levels by recombinant luminescent bacteria. J Exp Bot **56:** 695–702

Stonebloom S, Burch-Smith T, Kim I, Meinke D, Mindrinos M, Zambryski P (2009) Loss of the plant DEAD-box protein ISE1 leads to defective mitochondria and increased cell-to-cell transport via plasmodesmata. Proc Natl Acad Sci USA **106:** 17229–17234

Tucker JE, Mauzerall D, Tucker EB (1989) Symplastic transport of carboxyfluorescein in the staminal hairs of *Setcreasea purpurea* is diffusive and includes loss to the vacuole. Plant Physiol **90:** 1143–1147

Zambryski P (2008) Plasmodesmata. Curr Biol **18:** R324–325

Zhu T, Lucas WJ, Rost TL (1998) Directional cell-to-cell communication in the Arabidopsis root apical meristem: I. An ultrastructural and functional analysis. Protoplasma **203:** 35–47